Supernova Relic Neutrinos in Liquid Argon detectors

A.G. Cocco, A. Ereditato, G. Fiorillo, G. Mangano and V. Pettorino§

Dipartimento di Scienze Fisiche, Università di Napoli "Federico II",
and INFN, Sezione di Napoli,
Complesso Universitario di Monte Sant'Angelo, Via Cintia, I-80126 Napoli, Italy

Abstract. We study the possibility of detecting the background of Supernova Relic Neutrinos (SRN) with liquid Argon Time Projection Chamber (TPC) detectors. As far as this study is concerned, these experimental devices are mainly sensitive to electron neutrino signals, and could provide further information on both Supernova explosion mechanism and star formation rate at redshifts $z \leq 1$. We study in details the main contributions to background in the relevant energy range from ^{8}B and *hep* solar neutrinos as well as from low energy atmospheric neutrino fluxes. Depending on the theoretical prediction for the SRN flux we find that for a 3 kton and a 100 kton liquid Argon TPC detectors the signal may be observed at the 1σ and 4σ level, respectively, with 5 years of data taking.

PACS numbers: 13.15.+g, 97.60.Bw, 14.60.Pq

§ alfredo.cocco@na.infn.it
antonio.ereditato@na.infn.it
giuliana.fiorillo@na.infn.it
gianpiero.mangano@na.infn.it
valeria.pettorino@na.infn.it

1. Introduction

Type II Supernova explosions (SNII) are among the most energetic events in the Universe known so far. Massive stars with mass larger than about eight solar masses undergo several burning phases until the compact core has been fused into iron. Lacking any further source of nuclear energy to balance gravity, the star collapses. When the inner core reaches nuclear densities an outward propagating shock wave is produced, which eventually leads to a huge luminosity release of the order of 10^{53} erg and to the explosion of the outer layers of the star. This huge energy flux is almost entirely in the form of neutrinos of all flavors produced via weak processes which diffuse through the very dense inner part of the structure and eventually freely escape from the neutrinosphere, cooling the remnant proto-neutron star on a time scale of 10 seconds.

This SNII model has been confirmed by the detection of neutrinos from the SN1987A [1, 2], though the small number of observed events still leaves important issues unsolved, as for example the shock revival mechanism, the way the flux is distributed among the neutrino and antineutrino flavors, and finally a detailed knowledge of the neutrino mean energies at the neutrinosphere. For a recent review on this and related issues see *e.g.* [3].

Future nearby SNII events would probably provide enough information to achieve a deeper understanding of the core-collapse mechanism, since many running experiments, such as Super-Kamiokande [4], SNO [5], KamLAND [6] and LVD [7], as well as others under construction, like ICARUS [8, 9, 10], will collect a huge number of neutrino events, of the order of 10^4. Waiting for such an event, whose rate is typically estimated to be of a few per century in our galaxy, it is interesting to study the possibility to detect with present and future experiments the isotropic neutrino flux due to all SNII that have occurred so far in the Universe. This would represent an independent probe of SNII mechanism, as well as of the SNII rate as a function of redshifts up to $z \sim 2$. The latter, being simply proportional to the star formation rate for stars heavier than $8M_\odot$, is an important cosmological observable that is presently studied via optical and UV surveys but that is still poorly known at high redshifts.

The expected Supernova Relic Neutrino (SRN) flux has been considered by several authors [11, 12, 13, 14, 15, 16, 17], and the results span quite a wide range, mainly because of different modelling of the star formation rate versus z. All these predictions but the one of the simplest constant supernova rate model [11] are compatible with the present experimental upper bound on $\bar{\nu}_e$ flux obtained by the Super-Kamiokande Collaboration, $\Phi(\bar{\nu}_e) < 1.2$ cm^{-2}s^{-1} for neutrino energies higher than 19.3 MeV [18]. A forecast for future possible detection of the signal in this experiment, as well as in KamLAND, has been considered in [19]. The authors find that, by adopting a model which is still compatible with the Super-Kamiokande bound and which is also motivated by UV density studies and by the Sloan Digital Sky Survey cosmic optical spectrum bounds on the z behavior of the star formation rate [20, 21], the SRN background may be detected at the 1σ level in a few years running. Furthermore, it has been recently

pointed out that the addition of a small fraction of gadolinium trichloride in water Cherenkov detectors would strongly lower the background below 18 MeV [22], since radiative neutron capture by Gd would allow antineutrino tagging by the coincidence detection of the reaction $\bar{\nu}_e + p \rightarrow e^+ + n$. Modifying Super-Kamiokande detector in this way would lead to a possible detection of SRN at least at 1σ with less than one year of further data (see [19] and References therein).

In this paper we consider the possibility of measuring the SRN signal by using a different class of experiments based on the liquid Argon TPC (Time Projection Chamber) technique [23]. Presently, this experimental method is adopted in the ICARUS experiment whose final 3 kton configuration (T3000) is planned to be commissioned at the INFN Gran Sasso Underground Laboratories in the near future [8]. We note that large mass liquid Argon TPC detectors (100 kton) have been also considered as powerful experimental devices for next generation neutrino physics and in particular as SNII neutrino flux detectors [24].

Though with different efficiencies, experiments like ICARUS are sensitive to all neutrino flavors. As we will discuss in Section 3, neutrinos and antineutrinos interact via neutral current with Argon nuclei, as well as by elastic scattering off electrons. Electron neutrinos can also undergo charged current interactions, which indeed are the leading processes with the highest cross section. Electron antineutrino charged current interactions are typically at least one order of magnitude smaller. It is worth stressing that the SRN signal would be mainly detected in this case in its ν_e component, so that ICARUS-like experiments provide a complementary piece of information with respect to Super-Kamiokande or KamLAND, which instead constrain the $\bar{\nu}_e$ flux. The present bound on low energy ν_e steady flux comes from the Mont Blanc Laboratory, $\Phi_{\nu_e} \leq 6.8 \cdot 10^3$ cm^{-2} s^{-1} in the energy range $25 \div 50$ MeV [25]. As we will see in the following a liquid Argon TPC experiment like ICARUS might improve this result by several orders of magnitude.

The main background sources for SRN events, in the relevant neutrino energy range of $10 \div 50$ MeV, are given by solar and low energy atmospheric neutrinos. These fluxes are indeed large enough to completely overwhelm the SRN signal at low energies, lower than the ^{8}B neutrino flux endpoint at approximately 16 MeV, as well as for sufficiently high energies where the atmospheric neutrino flux becomes the dominant contribution. However, in the intermediate energy range of $16 \div 40$ MeV the expected SRN signal is likely to represent a substantial fraction of the total flux. By suitably choosing the energy window, fluxes as the one considered in [19] may therefore be detectable.

This paper is organized as follows. In Section 2 we review the main features of SRN fluxes and we introduce the fiducial model used in our analysis. Section 3 covers the neutrino interaction processes in liquid Argon TPCs. The results of our simulation are reported in Section 4, where the expected energy spectrum and event rate from SRN are studied as a function of the star formation rate and the effect of the resonant neutrino oscillations in the outer Supernova matter layers. We also discuss there the backgrounds from solar and atmospheric neutrinos, as well as other possible sources of background,

comparing them with the SRN flux. Finally, we report our conclusions in Section 5.

2. Supernova Relic Neutrino flux

The neutrino differential flux $\Phi_\alpha(E_\nu)$ (number of neutrinos per energy interval, per unit time and per unit area) from past SNII exploded in our observable Universe can be written as follows:

$$\Phi_\alpha(E_\nu) = c \int_0^{z_{max}} \frac{dz}{H(z)} R_{SN}(z) \langle N_\alpha(E_\nu(1+z)) \rangle \quad , \tag{2.1}$$

where α denotes the neutrino or antineutrino flavor and $H(z)$ is the Hubble parameter

$$H(z) = H_0 \left(\Omega_m (1+z)^3 + \Omega_\Lambda + \Omega_R (1+z)^4 + (1 - \Omega_m - \Omega_\Lambda - \Omega_R)(1+z)^2 \right)^{1/2} \quad . \tag{2.2}$$

Since SNII produce equal fluxes for μ and τ neutrinos/antineutrinos, in the following we will collectively denote these states as ν_x and $\bar{\nu}_x$. In Equation (2.2) $H_0 = 100\, h$ km s^{-1} Mpc^{-1} is the present value of the Hubble parameter, with $h = 0.7\pm0.1$ [26, 27], while R_{SN} in Equation (2.1) is the SNII rate per unit time and comoving volume and $\langle N_\alpha \rangle$ is the number of ν_α emitted per unit of initial unredshifted energy by a SNII averaged over the stellar initial mass function and evaluated at $E_\nu(1+z)$, where E_ν is the energy measured on earth.

In the following we consider a spatially flat ΛCDM model with $\Omega_m = 0.3$, $\Omega_\Lambda = 0.7$ and $\Omega_R \sim 0$. The value of z_{max} is typically set by the experimental threshold on the lowest detectable neutrino energy. In fact, with increasing z the energy of neutrinos at production, which is typically of order of 10 MeV, is redshifted towards smaller values which eventually become difficult to be measured.

The Supernova rate $R_{SN}(z)$ is the star formation rate for stellar masses larger than 8M$_\odot$. Several models have been considered in the recent literature [11, 12, 13, 14, 15, 16, 17], whose predictions for the neutrino flux vary by approximately one order of magnitude. For our analysis we will consider a fiducial model as in [19]

$$\begin{aligned} R_{SN}(z) &= R_0 (1+z)^\beta, & z \leq 1 \\ &= R_0\, 2^{\beta-\alpha} (1+z)^\alpha, & z > 1 \quad , \end{aligned} \tag{2.3}$$

where the present rate R_0 is estimated in the range $(0.7 \div 4) \cdot 10^{-4}$ yr^{-1} Mpc^{-3} [20]. Limits on the slope parameters have been found in [21] using the Sloan Digital Sky Survey optical spectrum giving the ranges $2 \leq \beta \leq 3$ and $0 \leq \alpha \leq 2$. In particular, all our results given in the following are obtained using $R_0 = 2 \cdot 10^{-4}$ yr^{-1} Mpc^{-3}, $\beta = 2.5$ and $\alpha = 1$. This choice corresponds to an electron antineutrino flux which saturates the Super-Kamiokande bound [18]. As suggested by [19], such SRN flux could be detected by Super-Kamiokande in the near future. In this case, the measurement of the electron neutrino event rate by a future LAr experiment, compared to the predictions discussed in the following, would provide an important check of the core-collapse SNII model, in particular of the ν_e versus $\bar{\nu}_e$ flux properties.

Corresponding estimates for higher or lower values of R_0 can be obtained straightforwardly, since this parameter linearly enters the neutrino differential flux. We

also discuss in the following how our findings are affected when both the parameters α and β vary in the ranges shown above.

The second important input of Equation (2.1) is the neutrino spectrum emitted by a SNII, which should be averaged over the mass distribution. Actually, all relevant properties which characterize the neutrino spectrum are only weakly depending on the mass of the star, at least for not very heavy stars. We will therefore make the assumption that the mass average can be approximated by the neutrino spectrum of a *typical* Supernova. This spectrum is obtained by numerically solving the explosion dynamics [3] and can be parameterized with good accuracy by a Fermi-Dirac distribution

$$N_\alpha(E_\nu) = k_\alpha \frac{\mathcal{L}_{SN}}{T_\alpha^4} \frac{E_\nu^2}{\exp(E_\nu/T_\alpha - \eta_\alpha) + 1} \quad , \tag{2.4}$$

where $\mathcal{L}_{SN}$ is the Supernova luminosity, T_α the effective ν_α temperature and η_α is usually known as *pinching* parameter. Finally, the constant k_α is chosen so that the first momentum of the distribution is normalized to the total energy emitted in the ν_α channel. Typical values for these parameters, which will be adopted in our study, are the following

$$T_{\nu_e} = 3.5 \, MeV, \quad T_{\bar{\nu}_e} = 5 \, MeV, \quad T_{\nu_x} = 8 \, MeV \quad ,$$
$$\eta_{\nu_e} = 2, \quad \eta_{\bar{\nu}_e} = 2, \quad \eta_{\nu_x} = 1 \quad . \tag{2.5}$$

We consider a total luminosity $\mathcal{L}_{SN} = 3 \cdot 10^{53}$ erg that is equally distributed among the neutrino/antineutrino species.

Neutrino fluxes from a SNII as measured on earth are influenced by oscillation phenomena. Once produced at neutrinosphere, neutrinos propagate in the outer star layers and experience two MSW resonances at different densities (see *e.g.* [28]). The first resonance governed by atmospheric mass splitting and the value of the small mixing angle θ_{13} occurs at 10^3 g cm^{-3} (10 MeV/E$_\nu$). At a lower density of 10^2 g cm^{-3} (10 MeV/E$_\nu$) a second resonance takes place determined by the solar parameters Δm_{12}^2 and θ_{12}. For the experimentally favored Large Mixing Angle (LMA) solution of the solar neutrino problem this second resonance satisfies the adiabatic condition for all realistic matter profiles in a SNII. On the other hand, depending on the neutrino mass hierarchy and the value of θ_{13}, the higher density resonance occurs in the neutrino or in the antineutrino sectors and can be fully adiabatic or rather maximally violating adiabaticity. Correspondingly, the survival probabilities take different values, as shown in Table 1 where we consider the two limiting cases of large and small θ_{13} mixing angle, $\sin^2 \theta_{13} \geq 10^{-3}$ and $\sin^2 \theta_{13} \leq 10^{-6}$, respectively. For intermediate values of θ_{13} the survival probability depends on neutrino/antineutrino energy, but this effect is completely negligible for the SRN neutrino flux detection we are interested in, which is only weakly sensitive to the value of θ_{13}.

The effect of oscillations on SRN event will be discussed in the following. We use the LMA solution for solar neutrino problem which gives as best value $\sin^2 \theta_{12} = 0.3$ [29]. Since ν_x are produced with a higher mean energy we expect that in case I, which implies that all detected ν_e were born at neutrinosphere as ν_x, the number of SRN events would

	mass hierarchy	θ_{13}	$P(\nu_e \rightarrow \nu_e)$	$P(\bar{\nu}_e \rightarrow \bar{\nu}_e)$
I	normal	large	$\sin^2 \theta_{13}$	$\cos^2 \theta_{12}$
II	inverted	large	$\sin^2 \theta_{12}$	$\sin^2 \theta_{13}$
III	normal/inverted	small	$\sin^2 \theta_{12}$	$\cos^2 \theta_{12}$

Table 1. The ν_e and $\bar{\nu}_e$ survival probability due to MSW resonances in a SNII, as function of neutrino mass hierarchy and θ_{13} mixing angle.

be larger. In fact, the cross section for charged current interaction of ν_e with Argon nuclei, which is the leading interaction channel, grows with energy more rapidly than neutrino energy to the first power. The two scenarios II and III give instead very close results.

3. Neutrino detection with Liquid Argon TPC detectors

Neutrinos interact in liquid Argon TPCs via charged and neutral current interactions off Argon nuclei, as well as from elastic scatterings on atomic electrons, as described in the following along with Liquid Argon TPC detection capabilities.

3.1. CC interactions

Electron neutrino charged current interactions on Argon

$$\nu_e + {}^{40}\text{Ar} \rightarrow {}^{40}\text{K}^* + e^- \quad , \tag{3.1}$$

proceed via the creation of an excited state of ${}^{40}\text{K}$ and its subsequent gamma decay. The threshold for this process is given by the sum of the known Q-value of the inverse reaction (beta decay of ${}^{40}\text{K}$, $Q = 1.505$ MeV) and the energy needed to produce the given excited state of the ${}^{40}\text{K}$. At low energy, as discussed in [30], the main contributions to the cross section are from a Fermi transition to the isobaric analog state (IAS) of ${}^{40}\text{K}^*$ and Gamow-Teller transitions to three low-lying ${}^{40}\text{K}^*$ states. Details on the transitions taken into account in this analysis are shown in Table 2.

The charged current interaction cross section at higher neutrino energies (30 MeV $< E_\nu < 100$ MeV) has been evaluated in [31] by using a Random Phase Approximation calculation. Levels up to J=6 have been taken into account. A plot of the cross section is shown in Figure 1.

A similar analysis of the $\bar{\nu}_e$ charged current process

$$\bar{\nu}_e + {}^{40}\text{Ar} \rightarrow {}^{40}\text{Cl}^* + e^+ \quad , \tag{3.2}$$

has also been carried out in [31]. This process has a higher neutrino energy threshold of 7.48 MeV. The corresponding cross section is also reported in Figure 1. Notice that charged current cross sections grow with neutrino energy more rapidly than E_ν to the first power.

Transition	Excitation level (MeV)	Branching Ratio (%)
Fermi	4.384	32.76
Gamow-Teller	3.798	13.69
Gamow-Teller	3.11	18.16
Gamow-Teller	2.73	28.94

Table 2. Nuclear excitation levels for ^{40}K used in the analysis. See [30] for further details.
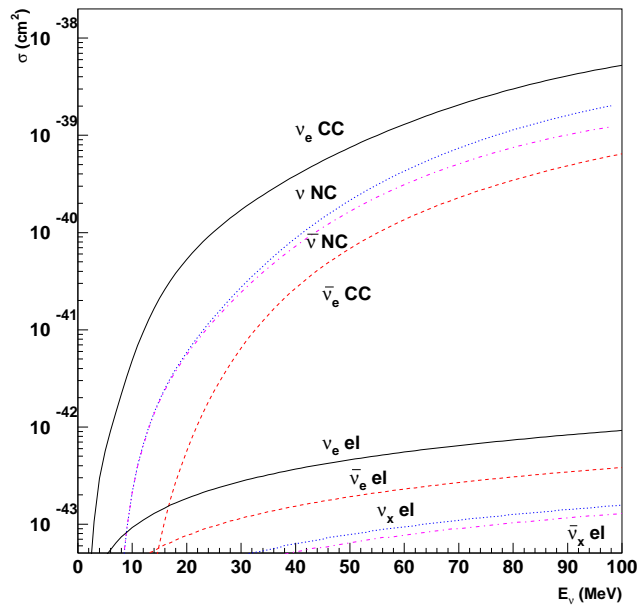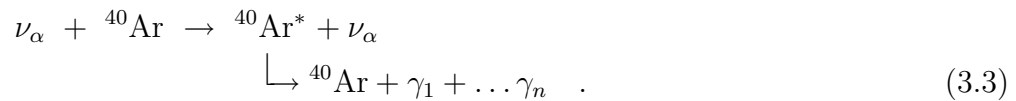

Figure 1. The cross section for neutrino interaction processes in liquid Argon. From top to bottom, charged current ν_eAr, neutral current ν_eAr, neutral current $\bar{\nu}_e$Ar, charged current $\bar{\nu}_e$Ar, and elastic scattering for ν_e, $\bar{\nu}_e$, ν_x and $\bar{\nu}_x$ on electrons. The neutral current results, which applies to all neutrino flavors, are from [10].

3.2. NC interactions

For relatively low energy transfers from the neutrino, neutral current reactions on Argon nuclei proceed via the excitation of nuclear resonances decaying back to Argon ground state with the emission of one or more photons

$$\nu_\alpha + {}^{40}\text{Ar} \rightarrow {}^{40}\text{Ar}^* + \nu_\alpha$$
$$\hookrightarrow {}^{40}\text{Ar} + \gamma_1 + \ldots \gamma_n \quad . \tag{3.3}$$

A study of nuclear levels of Argon reveals that the most energetic photon emitted in this process has an energy not exceeding 11 MeV [32]. These photons typically produce Compton electrons or electron/positron pairs, which however have energies lying outside the energy range we are interested in. In fact, as we will see in the following, the SRN

signal to background ratio is expected to be maximal by selecting the outgoing electron (positron) energy range above the threshold given by the steep rising of ^{8}B solar neutrino flux, at approximately 16 MeV. We also note that there is experimental evidence for a giant quadrupole resonance at 17.7 MeV [32], which is likely to produce multi-photon transition to ground state. In this case too, de-excitation of Argon would produce electrons with energy smaller than 16 MeV. Finally, for higher excitation energies, Argon nuclei are no longer stable and the final state contains one or more nucleons and a remnant nucleus, which can be distinguished from a single outgoing electron signal in liquid Argon TPC. As a consequence, in the following we will not consider neutral current interactions.

3.3. ES interactions

In our study we also consider neutrino elastic scattering, whose cross sections, shown in Figure 1, have a linear dependence on neutrino energy E_ν

$$\sigma(\nu_e e^- \to \nu_e e^-) \quad = 9.20{\cdot}10^{-45}(E_\nu/\text{MeV}) \text{ cm}^2 \quad , \tag{3.4}$$

$$\sigma(\bar{\nu}_e e^- \to \bar{\nu}_e e^-) \quad = 3.83{\cdot}10^{-45}(E_\nu/\text{MeV}) \text{ cm}^2 \quad , \tag{3.5}$$

$$\sigma(\nu_{\mu,\tau} e^- \to \nu_{\mu,\tau} e^-) = 1.57{\cdot}10^{-45}(E_\nu/\text{MeV}) \text{ cm}^2 \quad , \tag{3.6}$$

$$\sigma(\bar{\nu}_{\mu,\tau} e^- \to \bar{\nu}_{\mu,\tau} e^-) = 1.29{\cdot}10^{-45}(E_\nu/\text{MeV}) \text{ cm}^2 \quad . \tag{3.7}$$

Notice that the above cross sections are about three orders of magnitude smaller than the one for ν_e CC interactions. As we will see in the following, elastic scattering gives a very small contribution to the total SRN neutrino event rate in liquid Argon detectors.

3.4. Event detection

With the exception of neutral currents, all the processes considered above include one electron (or positron) in the final state and typically one or more photons. The final state is thus mainly electromagnetic. The excellent properties of liquid Argon as an electromagnetic calorimeter medium allow to detect energies down to a few hundreds of keV, therefore no energy threshold has been considered in our analysis.

In this paper we will refer in particular to the ICARUS detector that combines the features of a bubble chamber as far as the spatial resolution and the particle identification are concerned, to those of an electronic TPC. The detector is continuously active and sensitive, self-triggering and able to perform high-quality imaging even of low energy events such as those due to the interaction of neutrinos from stellar collapses [8].

We will assume in the following that electrons above 5 MeV can be measured with full efficiency in the detector, despite the presence of de-excitation photons. The latter could be possibly used to improve the knowledge of the incoming neutrino energy. As reported in [33], the electromagnetic energy resolution in ICARUS TPC can be parametrized as follows

$$\frac{\sigma(E_e)}{E_e} = \frac{11\%}{\sqrt{E_e(\text{MeV})}} + 2.5\% \quad , \tag{3.8}$$

in the neutrino energy range relevant for our analysis.

4. SRN signal and backgrounds

There are two main sources of background for the SRN signal in the energy range $10 \div 50$ MeV. For energies lower than approximately 20 MeV the (largely) dominant contribution comes from ^{8}B and *hep* solar neutrinos. These fluxes are quite accurately known. In Figure 2 we show the results of the standard solar model by Bahcall and Pinsonneault [34]. Total fluxes are chosen according to the best values suggested in [34], namely $\Phi_B = 5.79 \, (1\pm0.23) \cdot 10^6$ cm^{-2} s^{-1} and $\Phi_{hep} = 7.88 \, (1\pm0.16) \cdot 10^3$ cm^{-2} s^{-1}, while the energy profile has been obtained with the data given in [35] (see also [36]). The ^{8}B flux is dominating the ν_e flux up to an energy of 15 MeV, while *hep* neutrino flux extends well beyond, up to 18.8 MeV.
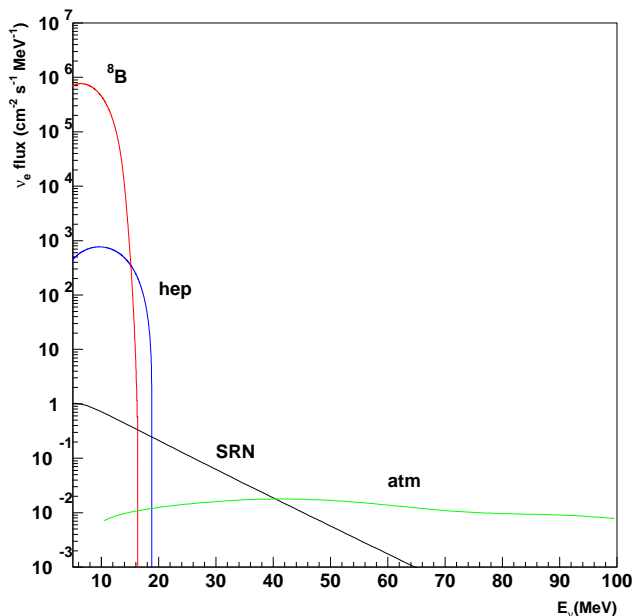

Figure 2. The expected SRN flux of ν_e for the model of Section 2, a normal neutrino mass hierarchy and $\sin^2 \theta_{13} = 0.02$. The ^{8}B and *hep* solar fluxes are also shown together with the atmospheric ν_e flux. All fluxes are shown versus the neutrino energy.

At higher energies the atmospheric neutrino background becomes dominant. The estimated flux for ν_e down to an energy of 10 MeV at the underground Gran Sasso Laboratory is shown in Figure 2 [37], as predicted by the FLUKA Monte Carlo package [38]. There is a systematic error in the evaluation of the atmospheric neutrino flux, due to uncertainties both in the absolute flux of primary cosmic rays producing neutrinos and in the cross section for hadronic interactions. We assume in the following a 30% relative uncertainty as a conservative estimate for these systematic effects [37].

Assuming the reference model considered in Section 2, we find an interesting energy window where the SRN signal can be detected, at least in principle. From Figure 2 we notice that from the *hep* endpoint at 19 MeV up to energies as high as 40 MeV the SRN ν_e give a relevant contribution to the total expected flux. Actually, this prediction strongly depends on the estimated SRN flux. For those models which predict a lower flux this energy window can become much smaller or even disappear. In any case, we see that any attempt to detect the SRN signal, in particular in its ν_e component, requires a preliminary analysis of the possible signal to background ratio in the $20 \div 40$ MeV energy range.

Other possible backgrounds have been considered:

(i) Electrons coming from the decays of low momentum muons produced in the interactions of atmospheric $\nu_\mu/\bar{\nu}_\mu$ and escaping detection before the decay vertex ("invisible muons"), could mimic neutrino interactions in the target. This is an irreducible background in experiments like Super-Kamiokande, where muons with kinetic energy lower than 50 MeV are below threshold for emitting Cherenkov photons. Differently from water Cherenkov detectors, LAr TPCs do not suffer from this background, being able to detect very low energy tracks, down to a few hundreds of keV. Furthermore, in these detectors the decay of a $\mathcal{O}(20$ MeV) momentum muon results into an event topology that can be easily disentangled from a signal event (see for example [33]). These events in fact present a high charge density at the beginning of the track due to the high ionization of the muon at the end of its range.

(ii) Beta decays following spallation by cosmic ray muons has also been investigated as a source of background. Among possible spallation products the highest decay energies have been found to be less than 10 MeV (^{36}P β^- decay), well below the lower energy cut used in the following analysis for SRN searches with LAr detectors. These processes, thus, do not represent a possible source of background. It is worth pointing out that the very good electromagnetic energy resolution of ICARUS-like detectors (6% at 14 MeV [33]) allows for an accurate measurement of the visible energy, which is not the case for water Cherenkov detectors in the same energy range. Finally we also notice that, since LAr detectors are fully sensitive to any incoming charged particle, there is no chance for muon spallation inside the detector to produce the signature of a single low energy electron.

(iii) Nuclear recoils arising from the NC atmospheric neutrino interactions and from the scattering of fast neutrons coming from the surrounding materials could be misidentified due to quenching in LAr. We notice that a significant recombination is possible for highly charged heavy particles in presence of electric fields of the order of 0.5 kV/cm [39]; however, the largest Argon nucleus recoil kinetic energy for a scattering with a fast neutron is $E_{\text{recoil}} = 4E_{\text{n}}A/(A+1)^2$ where A=40. This means that, assuming a 60% quenching, a 1 GeV neutron is needed to produce a recoil of 50 MeV, quenched to 20 MeV. At this energy scale for the incident particle,

inelastic scattering processes take place and the outgoing fragments are visible in a LAr detector. In addition, the different range out properties of a nuclear recoil and of an electron would result in events of very different topologies.

For the above considerations, the only sources of background included in our analysis are solar and atmospheric neutrino induced events.

4.1. MonteCarlo simulation

We have simulated 10^4 SRN events according to a SNII spectrum whose parameters are chosen as in Equation (2.5) along with 10^4 and 10^5 solar and atmospheric neutrino events, respectively. Incoming neutrino spectra have been normalized to the expected fluxes. The SRN flux has been normalized according to [19]. We consider a normal neutrino mass hierarchy and a large value for the θ_{13} mixing angle (case I of Table 1). Interaction of these fluxes with the detector proceeds via charged current and elastic scattering as described before. We use as detection signature the electron (positron) produced in the charged current interaction, or the recoil electron for elastic scattering. The electron energy E_e spectrum is produced by using the corresponding differential cross section $d\sigma/dy$, where y is the fraction of the incoming neutrino energy carried by the scattered electron ($y = E_e/E_\nu$). For CC events we take into account the thresholds and detection efficiency described in Section 3. All results are reported in terms of the electron/positron *measured* energy. For this purpose, the energy resolution of the detector reported in Equation 3.8 has been taken into account.

Results are shown in Figure 3, where the number of events due to solar, atmospheric and SRN neutrinos is given as a function of the electron (positron) energy, in the energy window $10 \div 50$ MeV. The signature of SRN neutrino induced events for $16 \leq E_e \leq 40$ MeV is more clearly seen in Figure 4 where we compare the total event energy spectrum with the one expected for the solar and atmospheric backgrounds only.

In Figure 5 we show the different contributions to the energy spectrum given by ν_e and $\bar{\nu}_e$ charged current interactions and elastic scattering, summed over all neutrino/antineutrino species. The plot shows that the SRN signal at an ICARUS-like detector is almost entirely due to ν_e charged current interactions.

A change of the values of α or β affects the expected signal quite differently. Since the solar neutrino background is too high for neutrino energies lower than 16 MeV, for a typical SNII spectrum and even in the best case of a maximal $\nu_x - \nu_e$ oscillation the contribution of all SNII at redshift larger than 1 cannot be detected. In fact, for a ν_x effective temperature at the neutrinosphere of 8 MeV, we estimate that for $z = 1$ a 15% fraction of the total ν_e flux produces electron charged current events with energy above the 16 MeV threshold, while this fraction is only 1% for $z = 2$ sources. This implies that the expected signal is very weakly depending on the star formation rate at redshift larger than 1. This feature is clearly seen in Figure 6 where we show how the SRN spectrum versus the electron (positron) energy changes when varying the star formation slope parameters. The dependence on β is more pronounced. The total
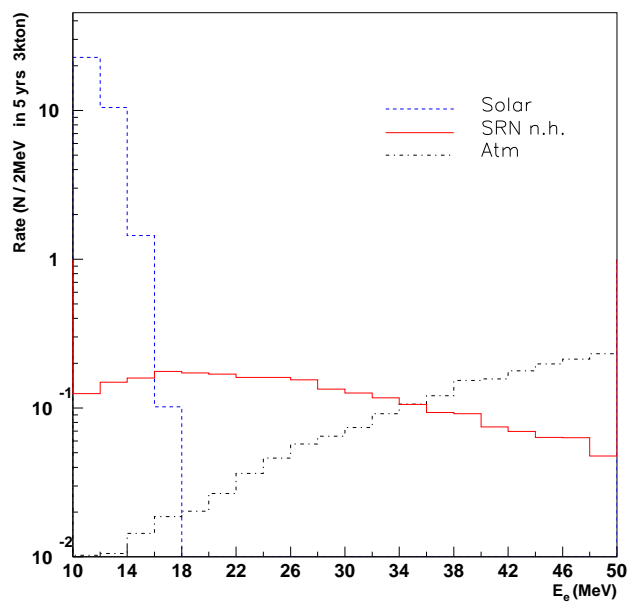
Figure 3. The simulated electron (positron) event spectrum due to solar neutrinos (blue dashed), atmospheric flux (black dot-dashed) and SRN neutrinos (red solid), versus the electron (positron) energy. A normal neutrino mass hierarchy (n.h.) and large θ_{13} is assumed. Results are for a 3 kton detector.
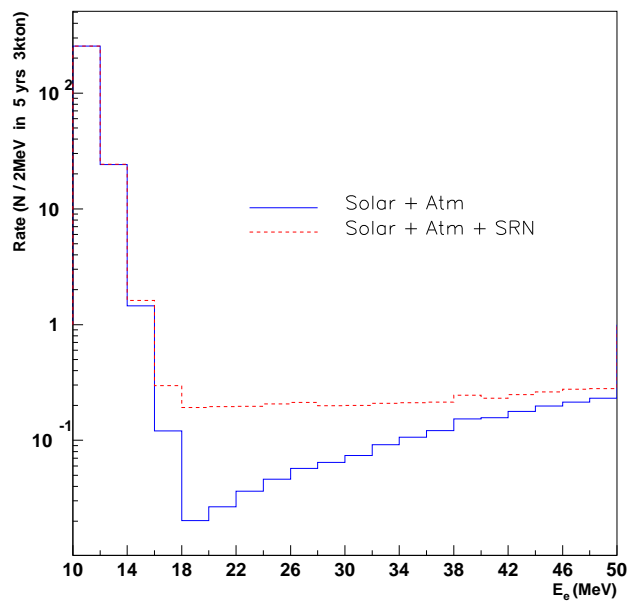

Figure 4. The total event spectrum compared to background due to solar plus atmospheric neutrinos for a 3 kton detector with a normal neutrino mass hierarchy and large θ_{13}.
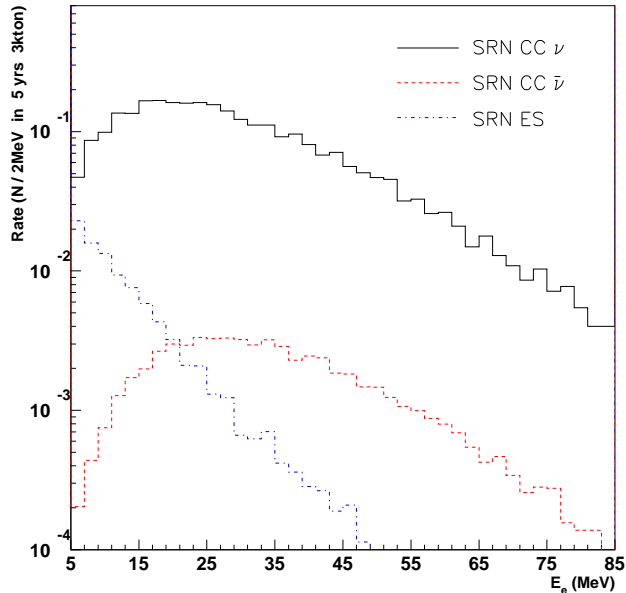
Figure 5. The relative contribution of ν_e charged current (black solid line), $\bar{\nu}_e$ charged current (red dashed) and elastic scattering summed over all neutrino species (blue dot-dashed) for each electron (positron) energy bin for a 3 kton detector.

number of SRN events changes by a factor $\pm 20\%$ with respect to the result for $\beta = 2.5$, when β varies in the range $2 \leq \beta \leq 3$.

4.2. Results

If one integrates the energy spectrum over the selected energy window for a 3 kton liquid Argon detector like ICARUS running for 5 years one obtains $N_{SRN} = 1.7$ events from SRN flux, to be compared with $N_{BG} = 0.9$ events from the solar and atmospheric neutrino background. To evaluate the error on the expected number of events we consider the events in each bin distributed according to Poisson statistics $\sigma_{stat}^2 = N_{SRN} + N_{BG}$ and we add in quadrature a systematic error σ_{syst} to account for a 30% uncertainty on the atmospheric flux normalization at low energies and the uncertainty on *hep* solar neutrino flux as given in [34]. We finally obtain $N_{SRN} = 1.7 \pm 1.6$, for $16 \, \text{MeV} \leq E_e \leq 40 \, \text{MeV}$

In case of no event detected and applying the approach described in [40] this would result in an upper limit on the SRN electron neutrino flux of

$$\Phi_{\nu_e} < 1.6 \ \text{cm}^{-2} \, \text{s}^{-1} \ \text{at } 90\% \text{ C.L.}$$

This limit would considerably improve the MontBlanc result [25]. The sensitivity of a LAr experiment like ICARUS is therefore close to the recently published Super-Kamiokande bound on the SRN electron antineutrino. The statistical significance of
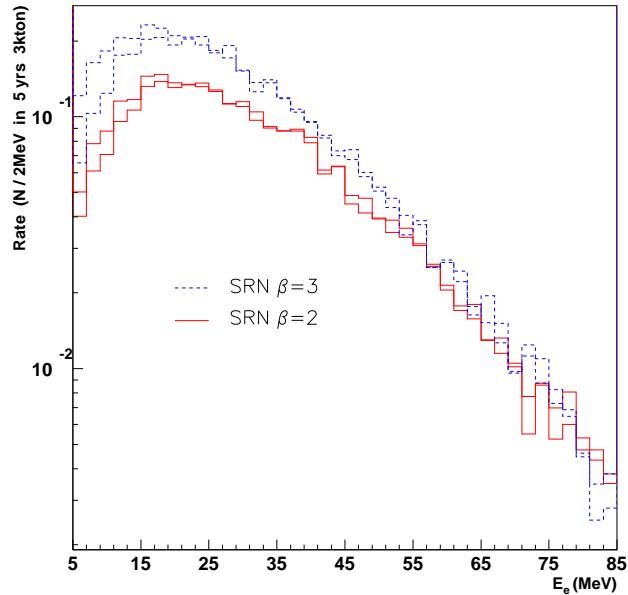
Figure 6. The dependence of the SRN signal on α and β as expected in a 3 kton detector. Upper (blue dashed) curves are for $\beta = 3$ and, from bottom to top, $\alpha = 0, 2$. The lower (red solid) curves are for $\beta = 2$ and the same values of α.

a positive observation would be greatly enhanced by using the full spectral information of the signal events.

The above result quite strongly depends on the selected energy window. If we try to push the lower bound towards lower energies the steep rise of the *hep* and ^{8}B neutrino events significantly raises the background. As an example, we find $N_{SRN} = 1.8$ and $N_{BG} = 2.4$ for $14\,\mathrm{MeV} \leq E_e \leq 40\,\mathrm{MeV}$. Similarly, a larger upper energy cut gives a less significant result, due to the larger atmospheric neutrino flux. For $16\,\mathrm{MeV} \leq E_e \leq 50$ MeV we find $N_{SRN} = 2$ and $N_{BG} = 2$ which is slightly better than the result obtained with a lower energy interval, since atmospheric neutrino flux growth with energy is not dramatic.

We note that due to the small number of signal events the total uncertainty is largely dominated by the statistical error, that contributes for 99% of the total error. The remaining 1% is given by the estimated uncertainty on the atmospheric neutrino flux. Therefore, we expect that a sensible improvement of the SRN detection capability of the liquid Argon TPC technique should come from a larger fiducial mass or a longer running time. Recently, ideas about next generation liquid Argon TPC detectors have been put forward [24]. Fiducial masses as large as $50 \div 100$ kton have been envisaged. In this case, for a 100 kton running for 5 years one would get a more than 4σ measurement of the SRN flux

$$N_{SRN} = 57 \pm 12, \quad 16\,\mathrm{MeV} \leq E_e \leq 40\,\mathrm{MeV} \quad , \tag{4.1}$$

for a normal neutrino mass hierarchy and a large θ_{13} and according to the fiducial model considered in this paper.

As a final remark we consider the effect of the different neutrino oscillation schemes summarized in Table 1. In Figure 7 we show the expected SRN event spectrum for normal mass hierarchy and large θ_{13} and for inverted mass hierarchy and/or small θ_{13}. In particular the expected event rate in the energy range $16 \div 40$ MeV for cases II and III is now $N_{SRN} = 43 \pm 12$. As expected, this value is smaller than for scenario I (Equation (4.1)), since the electron neutrino flux is shifted toward lower energies. We see that, provided the star formation rate is independently fixed by other observations, the different neutrino mass hierarchy may be distinguished by SRN observation at the level of 1σ.
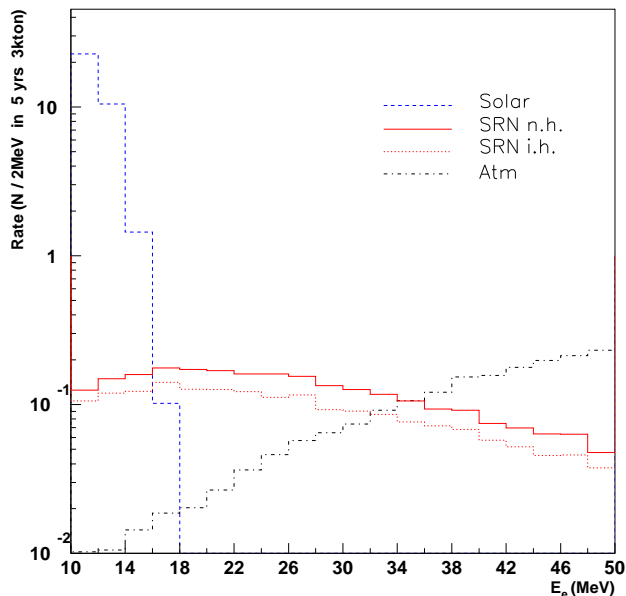

Figure 7. The electron (positron) spectrum for a neutrino normal mass hierarchy and large θ_{13} mixing angle (upper red solid curve) and for inverted mass hierarchy (i.h., lower red dotted curve) and/or small θ_{13}. The simulation is for a 3 kton detector.

5. Conclusions

In this paper we have studied the possibility of detecting the SRN flux signal at experiments like ICARUS, based on a liquid Argon TPC technique. In the relevant energy range, the leading interaction is the charged current ν_e scattering on Argon nuclei, which is revealed via the observation of the produced electron with full detection efficiency. In contrast with experiments such as Super-Kamiokande or KamLAND (which essentially detect the interactions of $\bar{\nu}_e$), the SRN flux would therefore be

constrained in the ν_e component by this experimental technique, which is thus to be considered as complementary to the cited ones.

The main detection problem is represented by competing backgrounds. Indeed, below 16 MeV the solar neutrino flux, in its ^{8}B and *hep* components, is larger than the expected SRN signal by orders of magnitude. Similarly, at high energies (>40 MeV) the atmospheric neutrino flux is largely dominating the total neutrino flux. Nevertheless, we have seen that, mainly depending on the star formation rate at $z \leq 1$ and more weakly on the neutrino oscillation pattern inside the SNII, there can be an electron energy window from 16 MeV to 40 MeV where the SRN neutrino flux is larger than backgrounds.

Using a reference model for SRN flux which is presently compatible with the experimental bound on $\bar{\nu}_e$ flux from relic SNII obtained by Super-Kamiokande, and which is also well motivated by astronomical observation, the SRN flux may be observed by a 3 kton detector like ICARUS at the 1σ level with five years of data taking. Because of the very few events expected in this case, the main source of uncertainty is due to the statistical error. A larger statistical significance will be obtained by next generation, large mass liquid Argon TPC detectors, reaching the level of 4σ for an exposure of 500 kton $\times$ yr.

Acknowledgments

References

[1] Hirata K *et al* 1987 *Phys. Rev. Lett.* **58** 1490
[2] Bionta R M *et al* 1987 *Phys. Rev. Lett.* **58** 1494
[3] Janka H T *et al* 2002 Explosion mechanisms of massive stars: a critical review of possibilities and perspectives *Preprint* astro-ph/0212314
[4] Super-Kamiokande Collaboration web page: http://www-sk.icrr.u-tokyo.ac.jp/doc/sk/index.html
[5] SNO Collaboration web page: http://www.sno.phy.queensu.ca/
[6] KamLAND Collaboration web page: http://www.awa.tohoku.ac.jp/html/KamLAND/
[7] Aglietta M *et al* 2002 *Nucl. Phys. Proc. Suppl.* **B110** 410
[8] Aprili P *et al* 2002 The Icarus Experiment: a second generation proton decay experiment and neutrino observatory at the Gran Sasso Laboratory *Preprint* CERN-SPSC-2002-027, CERN-SPSC-P-323. Web page: http://www.aquila.infn.it/icarus/
[9] Cavanna F, Costantini M L, Palamara O and Vissani F 2004 *Surveys High Energy Phys. 19* 35
[10] Gil-Botella I and Rubbia A 2004 *JCAP* **0408** 001
[11] Totani T, Sato K and Yoshii Y 1996 *Astrophys. J.* **460** 303
[12] Malaney R A 1997 *Astropart. Phys.* **7** 125
[13] Hartmann D H and Woosley S E 1997 *Astropart. Phys.* **7** 137
[14] Kaplinghat M, Steigman G and Walker T P 2000 *Phys. Rev.* **D62** 043001

[15] Ando S, Kato K and Totani T 2003 *Astropart. Phys.* **18** 307
[16] Ando S 2004 *Astrophys. J.* **607** 20
[17] Ando S and Sato K 2003 *Phys. Lett.* **B559** 113
[18] Malek M *et al* 2003 *Phys. Rev. Lett.* **90** 061101
[19] Strigari L *et al* 2004 *JCAP* **0403** 007
[20] Baldry I K and Glazebrook K 2003 *Astron. J.* **126** 1483
[21] Glazebrook K *et al* 2003 *Astrophys. J.* **587** 55
[22] Beacom J F and Vagins M R 2004 *Phys. Rev. Lett.* **93** 171101
[23] Rubbia C 1977 The Liquid Argon time projection chamber: a new concept for Neutrino Detectors
    Preprint CERN/77-08
[24] Ereditato A and Rubbia A 2004 Ideas for future liquid Argon detectors, to appear in *Proc. Third*
    International Workshop on Neutrino-Nucleus Interactions in the Few GeV Region, NUINT04
    (Gran Sasso)
[25] Aglietta M *et al* 1992 *Astropart. Phys.* **1** 1
[26] Freedman W L *et al* 2001 *Astrophys. J.* **553** 47
[27] Spergel D N *et al* 2003 *Astrophys. J. Suppl.* **148** 195
[28] Lunardini C and Smirnov A. Yu. 2003 *JCAP* **0306** 009
[29] Fogli, G L *et al* 2004 *Phys. Rev.* **D69** 017301
[30] Ormand W E, Pizzochero P M, Bortignon P F and Broglia R A 1995 *Phys. Lett.* **B345** 343
[31] Kolbe E, Langanke K, Martinez-Pinedo G and Vogel P 2003 *J. Phys.* **G29** 2569
[32] ENSDF Database 2004 web page: http://www-original.nndc.bnl.gov/nndc/ensdf/
[33] Amoruso S *et al* 2004 *Eur. Phys. J.* **C33** 233
[34] Bahcall J N and Pinsonneault M H 2004 *Phys. Rev. Lett.* **92** 121301
[35] Bahcall J N web page: http://www.sns.ias.edu/∼jnb/
[36] Bahcall J N *et al* 1996 *Phys. Rev.* **C54** 411
[37] Battistoni G private communication
[38] Fasso A, Ferrari A, and Sala P R 2000 *Proc. MonteCarlo 2000 Conference (Lisbon)* (Kling A,
    Barao F, Nakagawa M, Tavora L and Vaz P editors Springer-Verlag Berlin) 159;
    Fasso A, Ferrari A, Ranft J, and Sala P R 2000 ibidem 955
[39] Amoruso S *et al* 2004 *Nucl. Instr. Meth.* **A523** 275
[40] Feldman G J and Cousins R D 1998 *Phys. Rev.* **D57** 3873